THE JOURNAL OF PHYSICAL CHEMISTRY C

Article

pubs.acs.org/JPCC

Initial Decomposition Reactions of Bicyclo-HMX [BCHMX or *cis*-1,3,4,6-Tetranitrooctahydroimidazo-[4,5-*d*]imidazole] from Quantum Molecular Dynamics Simulations

Cai-Chao Ye,[†,‡] Qi An,[‡] William A. Goddard, III,[*,‡] Tao Cheng,[‡] Sergey Zybin,[‡] and Xue-hai Ju[†]

[†]Key Laboratory of Soft Chemistry and Functional Materials of MOE, School of Chemical Engineering, Nanjing University of Science and Technology, Nanjing 210094, P. R. China

[‡]Materials and Process Simulation Center, 139-74, California Institute of Technology, Pasadena, California 91125, United States

Supporting Information

ABSTRACT: We investigated the initial chemical reactions of BCHMX [*cis*-1,3,4,6-tetranitrooctahydroimidazo-[4,5-*d*]imidazole] with the following procedure. First we used density functional theory molecular dynamics simulations (DFT-MD) on the periodic crystal to discover the initial reaction steps. This allowed us to determine the most important reactions through DFT-MD simulations at high temperatures. Then we started with the midpoint of the reaction (unimolecular or bimolecular) from the DFT-MD and carried out higher quality finite cluster DFT calculations to locate the true transition state of the reaction, followed by calculations along the reaction path to determine the initial and final states. We find that for the noncompressed BCHMX the nitro-aci isomerization reaction occurs earlier than the NO_2-releasing reaction, while for compressed BCHMX intermolecular hydrogen-transfer and bimolecular NO_2-releasing reactions occur earlier than the nitrous acid (HONO)-releasing reaction. At high pressures, the initial reaction involves intermolecular hydrogen transfer rather than intramolecular hydrogen transfer, and the intermolecular hydrogen transfer decreases the reaction barrier for release of NO_2 by ~7 kcal/mol. Thus, the HONO-releasing reaction takes place more easily in compressed BCHMX. We find that this reaction barrier is 10 kcal/mol lower than the unimolecular NO_2 release and ~3 kcal/mol lower than the bimolecular NO_2 release. This rationalizes the origin of the higher sensitivity of BCHMX compared to RDX (1,3,5-trinitrohexahydro-1,3,5-triazine) and HMX (octahydro-1,3,5,7-tetranitro-1,3,5,7-tetrazocine). We suggest changes in BCHMX that might help decrease the sensitivity by avoiding the intermolecular hydrogen-transfer and HONO-releasing reaction.

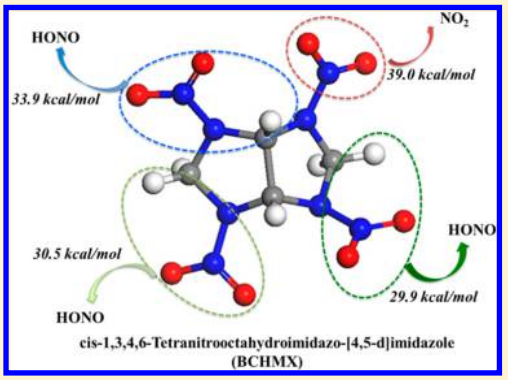

1. INTRODUCTION

cis-1,3,4,6-Tetranitrooctahydroimidazo-[4,5-*d*]imidazole was designed theoretically to have superior physical and energetic properties.[1,2] This molecule, which can be considered as bicyclo-HMX, is denoted as BCHMX. Following a very intense effort in the 1980s to find efficient and economic synthetic procedures to obtain larger amounts of BCHMX,[3,4] Zeman et al. in 2009 synthesized BCHMX and investigated the properties. The ignition temperature of BCHMX is 214−224 °C, compared to 204 °C for RDX (1,3,5-trinitrohexahydro-1,3,5-triazine) and 275 °C for *β*-HMX. The heat of explosion of BCHMX is 5.758 MJ/kg, which is approximately the same as pentaerythritol tetranitrate (PETN) (5.730 MJ/kg), but it is higher than for RDX (5.481 MJ/kg), and HMX (5.530 MJ/kg). In addition, the BCHMX melting point (268 °C) is much higher than PETN (141 °C) and RDX (204 °C) but slightly lower than HMX (275 °C).[5] BCHMX has a predicted maximum density of 1.86 g/cm^3, calculated detonation velocity of 9050 m/s, detonation pressure of 37 GPa, and maximum explosion heat of 6.518 MJ/kg.[5−7] Thus, BCHMX has the potential to be a good high-energy material. However, it has higher impact and electric-spark sensitivities, compared with RDX and *β*-HMX. In order to understand the origin of its high sensitivity we undertook to determine the mechanism with the expectation that this might provide clues to improve this material.

Although the synthesis,[8,9] properties, initiation reactivity,[10] and thermal behaviors[7] of BCHMX have been reported, the complex chemical behavior of BCHMX leaves many fundamental and practical issues to be understood. For instance, for high-energy materials, the initial thermal decomposition and reaction processes are essential in determining the energy release and detonation properties, as well as its sensitivity,[11−17] but the initial decomposition reaction of BCHMX has not been reported. For such normal nitro-based explosives as HMX and RDX, the early chemistry involves decomposition via a branching chain of radical reactions, with the activation energy determined by the

Received: October 13, 2014
Revised: January 5, 2015
Published: January 8, 2015

DOI: 10.1021/jp510328d
J. Phys. Chem. C 2015, 119, 2290−2296

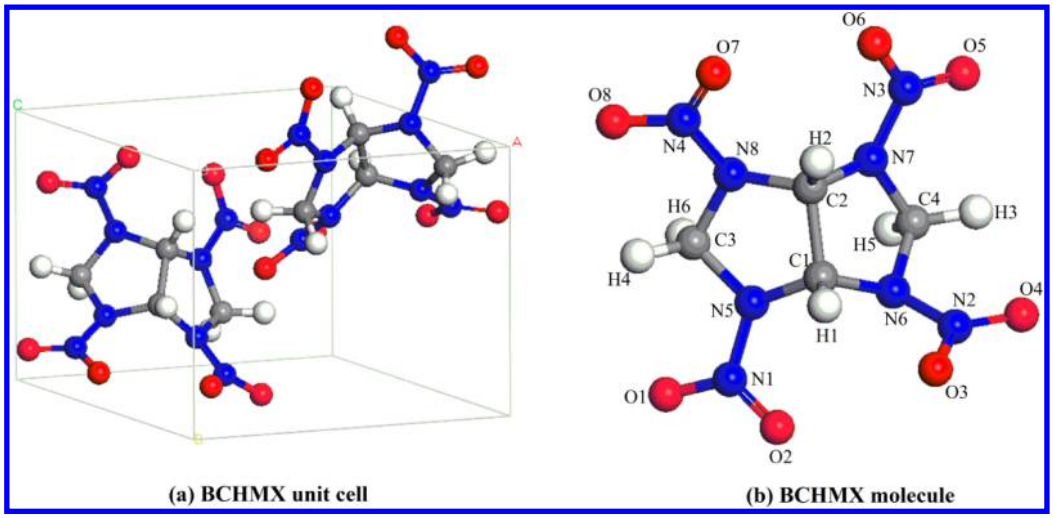

Figure 1. (a) Crystal structure and (b) molecular structure of *cis*-1,3,4,6-tetranitrooctahydroimidazo-[4,5-*d*]imidazole (BCHMX). The unit cell contains two BCHMX molecules. The C, H, O, and N are represented by grey, white, red, and blue balls, respectively.

unimolecular NO_2 cleavage.[18−22] In addition, intramolecular hydrogen transfer to produce nitrous acid (HONO) which decomposes to form HO and NO can compete with NO_2 cleavage as the first step of decomposition.[11,13,23,24] Since BCHMX has a molecular structure similar to RDX or HMX, but is much more sensitive, we were particularly interested in examining the first step of the decomposition mechanism of BCHMX.

In order to elucidate the initial reaction of BCHMX, we report here DFT-MD simulations using the forces from the PBE-ulg[25] flavor of DFT to examine the decomposition reaction of BCHMX. These studies on the initial reaction of BCHMX explain the relationship between initial reaction and sensitivities, and we suggest ways to improve its property.

2. METHODOLOGY

2.1. Density Functional Theory Molecular Dynamics Simulation (DFT-MD). Our DFT-MD simulations use interatomic forces calculated from quantum mechanics based on the PBE flavor of density functional theory (DFT)[26,27] in which exchange and correlation are described using the generalized gradient approximation (GGA), and London dispersion (van der Waals attraction) is treated by the low gradient correction.[25]

These periodic QM calculations were performed using the VASP package.[28−30] We found that a kinetic energy cutoff of 500 eV for the plane wave expansions gives excellent convergence of the total energies, energy differences, and structural parameters in structure optimization. The same energy cutoff was applied in the DFT-MD calculations. Only the gamma point of reciprocal space was sampled in the DFT-MD simulations. The convergence criteria were a 1×10^{-6} eV energy difference for solving the electronic wave function and 1×10^{-3} eV/Å force for structure optimization. For DFT-MD simulations, they were set to a 1×10^{-5} eV energy difference for solving the electronic wave function and a 1×10^{-3} eV/Å force. The spin-restricted KS solvers were used in the DFT-MD simulations, and the symmetry was not constrained.

The simulated system with eight molecules per periodic cell was obtained by replicating the unit cell (as shown in Figure 1) twice along the y and z directions. The structures were optimized before the DFT-MD simulations, as shown in Figure S1(a) of the Supporting Information (SI). To investigate the pressure effects on the initial reactions, we also performed simulations with the volume of the BCHMX unit cell compressed by 30%. This decreased the lattice constants $a \times b \times c$ from 8.59 Å × 7.07 Å × 8.75 Å to 7.86 Å × 6.73 Å × 7.03 Å with an initial external pressure of 20.0 GPa. This eight-molecule supercell is shown in Figure S1(b) (SI).

The DFT-MD simulation procedures were as follows. First the systems were heated at a constant rate from 20 to 300 K over 2 ps. Then the systems were equilibrated at 300 K for 1 ps using the NVT (constant volume, constant temperature, and constant number of atoms) ensemble. Finally, we heated the system from 300 to 3000 K uniformly over 20 ps. The time constant for the Nose−Hoover thermostat was 0.1 ps. The time step 1 fs was used for integrating the equation of motion. The high temperatures used in these simulations allowed many reactions to be observed within 20 ps of simulation. To analyze the fragments during the simulation, we used a bond length cutoff of 1.5 times of the normal bond length. These bond length cutoffs are shown in Table S1 of the SI.

2.2. Finite Cluster Calculation. To obtain accurate energetics, we extracted the molecules undergoing reactions from the trajectories of the periodic DFT-MD simulations. Then we located the nearby transition state, reactant, and product geometries in the gas phase at the level of PBE-ulg/6-31++G**, using Jaguar 8.2 transition states (TS) which were confirmed to have exactly one negative eigenvalue of the Hessian, which we followed by intrinsic reaction coordinate (IRC) scans to connect to the reactant and product structures. Thermodynamic properties were evaluated at 298.15 K and 1 atm. All gas-phase calculations were carried out using the Jaguar 8.2 package.[31]

3. RESULTS AND DISCUSSION

The DFT-MD simulations in this paper provide a very detailed, molecular-level description of the decomposition and reaction of condensed-phase BCHMX under various conditions. This information allowed us to extract valuable information about the complex chemistry involved, including unimolecular and multimolecular reactions.[15] Our goal is to elucidate the initial reaction pathway as BCHMX decomposes and describe the events in this high-energy material as it evolves to form

DOI: 10.1021/jp510328d
J. Phys. Chem. C 2015, 119, 2290−2296

intermediates that react with each other and with reactant to form eventually the final products observed theoretically. In this work, we focus on thermal decomposition of the condensed phase of BCHMX crystals, noncompressed BCHMX, and 30% compressed BCHMX and examine the initial reaction details under various conditions.

3.1. Reaction Mechanisms from DFT-MD. *3.1.1. Noncompressed BCHMX.* We first examined the initial decomposition reaction of noncompressed BCHMX. The molecular fragments during the cook-off simulation are plotted in Figure 2

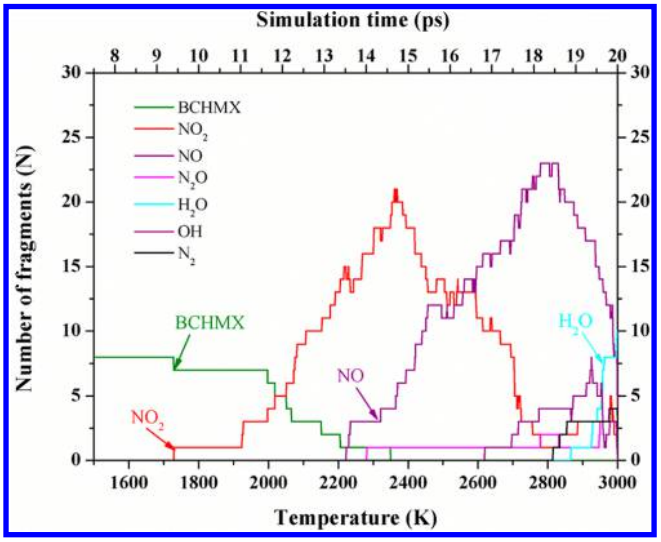

Figure 2. Species analysis for decomposition of noncompressed BCHMX heated from 300 to 3000 K over 20 ps. The first decomposition reaction for BCHMX occurs at ~1700 K (9.5 ps), releasing one NO_2 molecule. The second reaction occurs at 1910 K (11.0 ps) releasing two NO_2 dissociating from the decomposed BCHMX fragment.

as a function of temperature. The starting supercell consists of eight BCHMX molecules (208 atoms). The first reaction occurs as the temperature increases to ~1700 K at which point one BCHMX molecule experiences unimolecular decomposition, releasing the first NO_2 molecule, while the instantaneous pressure increased to ~1.0 GPa. Later at ~1900 K, more NO_2 molecules are released, as shown in Figure 2. Thus, we consider that unimolecular NO_2 cleavage is the initial reaction for noncompressed BCHMX. We will discuss the reaction mechanisms in more detail in the section describing the finite cluster calculations. As the temperature continued increasing above 2200 K, we observed secondary products, OH radical and N_2O, indicating decomposition of the ring.

To test whether the effect of the MD time step of 1 fs might be too long, we also used 0.25 fs time steps to do the noncompressed BCHMX cook-off simulation, as shown in Figure S4 (SI). We found that the initial reaction in noncompressed BCHMX remains the unimolecular NO_2 cleavage, indicating that the 1 fs time step is suitable for these BCHMX studies.

3.1.2. Precompressed BCHMX. To understand the initial chemical reactions under shock conditions where hotspot formation may play an essential role,[32−35] we also examined the initial reaction of BCHMX compressed by 30% volume as shown in Figure S1(b) (SI). This precompression leads to an initial external pressure of 20 GPa at 0 K. Using the compressed supercell containing 8 molecules and 208 atoms, we carried out DFT-MD as above. This leads to the results in Figure 3. Here we find that BCHMX molecules start to react at ~2050 K (12

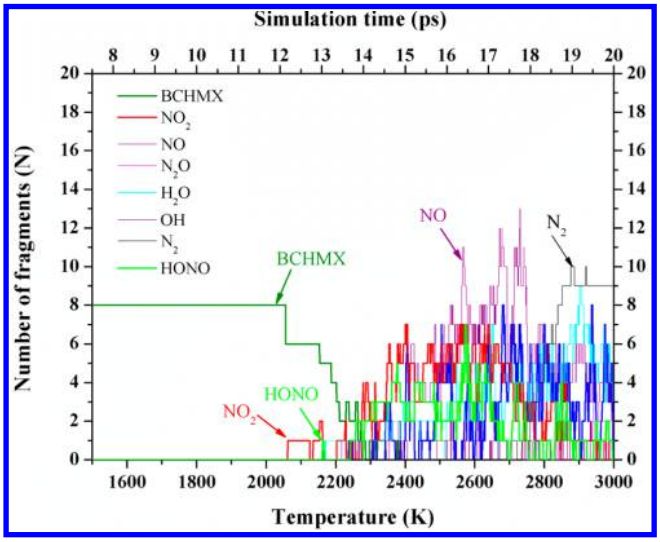

Figure 3. Species analysis for the decomposition of 30% compressed BCHMX heated from 300 to 3000 K over 20 ps. At ~2050 K (12 ps), two BCHMX molecules interact and release one NO_2 molecule, and then after another 1 ps (at ~2150 K), BCHMX molecules start decomposing one by one, releasing more NO_2 and HONO molecules.

ps, leading to an instantaneous pressure increase to ~22.0 GPa), involving both intermolecular hydrogen transfer and NO_2-releasing mechanisms. One hydrogen atom in a CH bond in BCHMX reacts with the N atom of the nearby BCHMX to form a N−H bond simultaneously with the first NO_2 released. Thus, the initial reaction in the compressed system is different from that for the noncompressed case. Then at ~2150 K (about 1 ps later), BCHMX molecules decompose one by one, releasing more NO_2 and HONO molecules, which is similar to the mechanism in RDX and HMX in which hydrogen transfer to/from HONO takes places at the beginning.[11,36,37]

3.2. Reaction Mechanism from Finite Cluster Calculations on Either the Single Molecule or the Dimer. To understand the nature of the initial decomposition reactions of noncompressed and compressed BCHMX, we extracted the activated intermediates from the condensed-phase simulation and analyzed the reaction mechanism as a gas-phase reaction.

The crystal structure for BCHMX has one long NN bond (1.427 Å) and three short NN bonds (1.355, 1.352, and 1.365 Å). We were surprised by the big differences and optimized the crystal structure using PBE-ulg where we find excellent agreement (bonds of 1.412, 1.364, 1.369, and 1.372 Å). Apparently these variations are related to the dihedral CNNO angle which should be 0 for the best resonance stabilization of the NO_2 with the ring N. Indeed the dihedral angle for the long bond is O3−N2−N6−C1 = 28.0°, whereas the other three are O6−N3−N7−C2 = 11.0°, O7−N4−N8−C2 = 12.5°, and O2−N1−N5−C1 = 10.5°. However, for the gas phase our calculations (PBE-ulg) lead to a symmetrical BCHMX molecule with C_2 symmetry where two N−N bonds (N1−N5 and N3−N7) are equal distance of 1.430 Å and the other two (N2−N6 and N4−N8) of 1.450 Å. The dihedrals O7−N4−N8−C2 and O3−N2−N6−C1 are equal to 26.4° and the other two dihedrals O2−N1−N5−C1 and O6−N3−N7−C2 to 20.6°. These results are compared in Table 1 with results for B3LYP

DOI: 10.1021/jp510328d
J. Phys. Chem. C 2015, 119, 2290−2296

Table 1. N−N Bond Distance and CNNO Dihedral Angle for All Four N−N Bonds of the BCHMX Molecule in the Condensed Phase (Experiment and PBE-ulg Level) and the Gas Phase (B3LYP, PBE, PBE-ulg Levels)

	condensed phase		gas phase[c]		
N−N bond and CNNO torsion	experiment[a]	PBE-ulg[b]	PBE-ulg	PBE	B3LYP
N1−N5 (Å)	1.365	1.364	1.430	1.430	1.400
N2−N6 (Å)	1.412	1.427	1.450	1.450	1.430
N3−N7 (Å)	1.355	1.369	1.430	1.430	1.400
N4−N8 (Å)	1.352	1.372	1.450	1.450	1.430
O2−N1−N5−C1 (deg)	16.2	10.5	20.6	20.2	16.9
O3−N2−N6−C1 (deg)	27.5	28.0	26.4	25.5	22.9
O6−N3−N7−C2 (deg)	14.8	11.0	20.6	20.2	16.9
O7−N4−N8−C2 (deg)	12.8	12.5	26.4	25.5	22.9

[a]Data from ref 5. [b]Data from crystal structure optimized by VASP in PBE-ulg level. [c]Data from molecular structure optimized by Jaguar in PBE-ulg, PBE, and B3LYP levels.

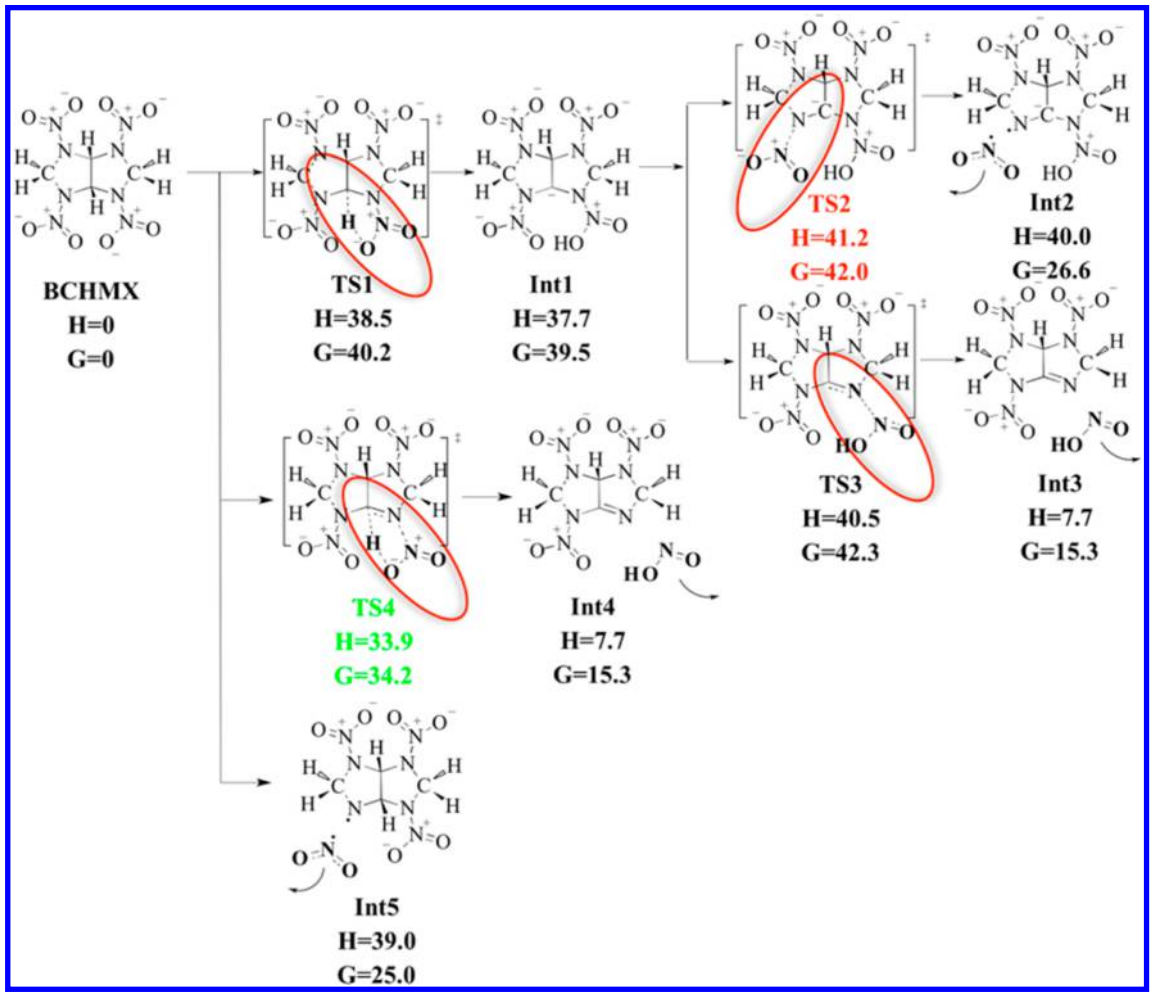

Figure 4. Mechanism of the first nitro-aci isomerization event and for the NO_2-releasing reactions from finite cluster calculations starting from the trajectory from the cook-off simulation of noncompressed BCHMX. The first step (**TS1** at 38.5 kcal/mol) is intramolecular hydrogen transfer within the BCHMX molecule, from CH to OH, which is followed quickly by NO_2 release (**TS2** at 41.2 kcal/mol). Configurations **TS1**, **Int1**, and **Int2** were extracted from the DFT-MD trajectory and then optimized as a gas-phase reaction, while **Int1**-**TS3**-**Int3** is a proposed reaction path to release HONO. The DFT-MD simulations also did not find the **TS4** to **Int4** pathway to release HONO, although the DFT finds this to have a barrier (**TS4**) of 33.9 kcal/mol, which is a lower barrier HONO releasing pathway in the gas phase. Unit is in kcal/mol.

which are similar. This big increase in NN is apparently due to the larger dihedrals in the gas phase.

First we considered the noncompressed periodic system, **BCHMX**-**TS1**-**Int1**-**TS2**-**Int2**, is the pathway extracted from the DFT-MD trajectory and then optimized as a gas-phase reaction. We found (see Figure 4) that the nitro-aci isomerization reaction to make the aci isomer of BCHMX **Int1** (at +37.7 kcal/mol) via **TS1**, in which one H atom of BCHMX transferred from the C atom to the nearby O atom, has a barrier of 38.5 kcal/mol, making it the rate-determining step (RDS). Starting with **Int1** the easiest pathway to eliminate the NO_2 molecule is breaking the N−N bond via **TS2** (at +41.2

DOI: 10.1021/jp510328d
J. Phys. Chem. C 2015, 119, 2290−2296

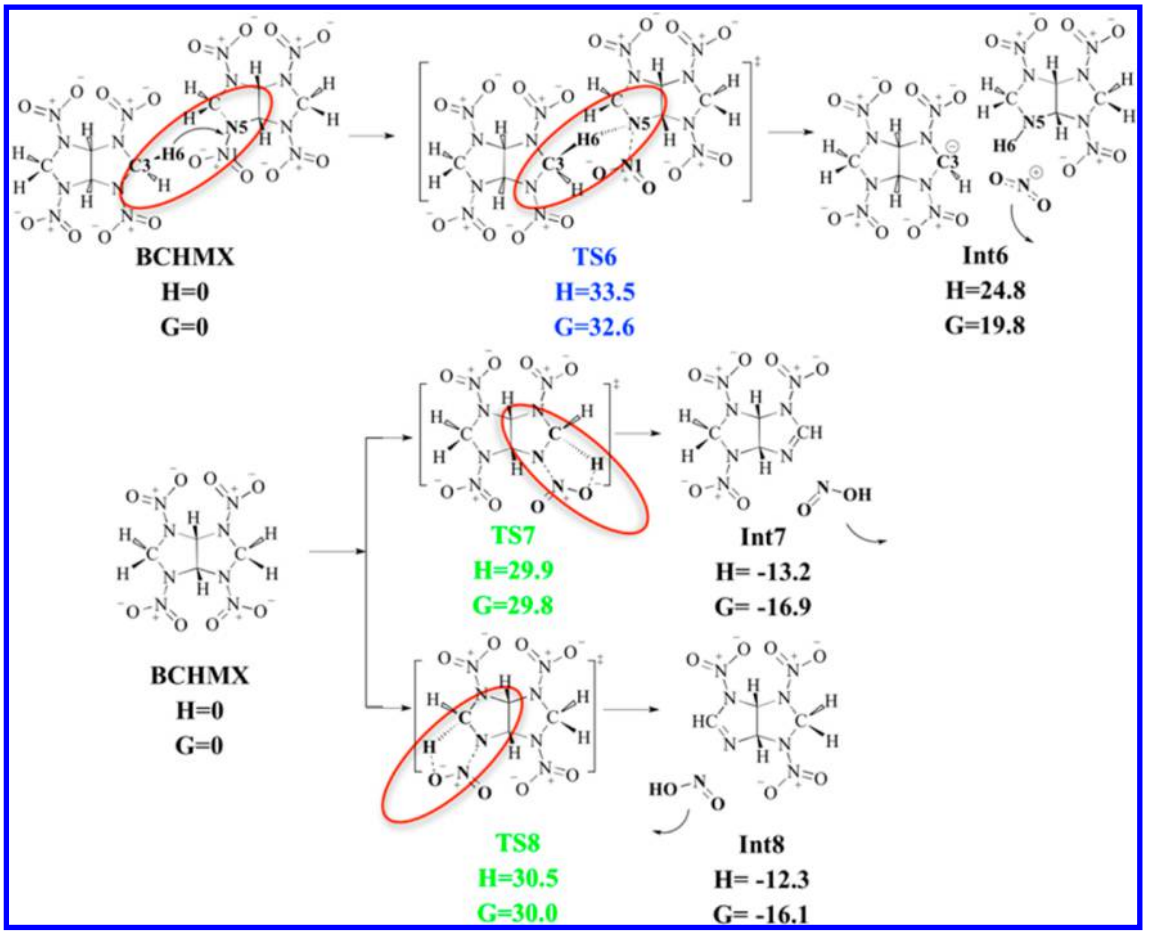

Figure 5. Mechanism of the first intermolecular hydrogen-transfer and NO_2-releasing reactions from finite cluster calculations starting from the trajectory from the cook-off simulation of compressed BCHMX. One hydrogen atom (H6) of the C3 atom in BCHMX reacts with the N atom (N5) of the nearby BCHMX to make a new N−H bond via **TS6**, followed by forming the N−H bond and the first NO_2 release. Configurations **TS6**, **Int6**, and **TS7** were extracted from the DFT-MD trajectory and then optimized as a gas-phase reaction. **BCHMX-TS8-Int8** is another possible path to release HONO calculated in the gas phase but not observed in the DFT-MD simulations. Unit is in kcal/mol.

kcal/mol) to form an intermediate **Int2** (shown in Figure 4), which we find to have a barrier of 3.5 kcal/mol above **Int1**.

Although BCHMX DFT-MD on the noncompressed period system did not find a HONO-releasing reaction in the first decomposition of BCHMX, the adiabatic QM calculations find two HONO-releasing pathways. One pathway stretches the N−N bond via **TS3** (at +40.5 kcal/mol) to release a HONO molecule, leading to a barrier of 2.8 kcal/mol above the aci isomer of BCHMX **Int1** (at +37.7 kcal/mol). The other pathway is for BCHMX to release HONO directly via **TS4**, with a barrier of 33.9 kcal/mol, which is lower than the barrier of the nitro-aci isomerization reaction. In the DFT-MD simulation for the noncompressed condensed phase the HONO-releasing reaction seems to be hindered by the nearby BCHMX molecule with a contact distance of 2.76 Å, whereas the $-NO_2$ that dissociates is ∼3.62 Å from the closest BCHMX (see Figure S3, SI). This seems to explain why HONO release was not observed in the fast heating rate MD simulation.

The reaction energy (barrier) for unimolecular NO_2 cleavage reaction without hydrogen transfer in BCHMX is calculated to be 39.0 kcal/mol (see Figure 4), which is 1.3 kcal/mol higher than the intramolecular hydrogen-transfer barrier, explaining why the intramolecular hydrogen-transfer first takes place before the unimolecular NO_2 cleavage reaction in MD simulation.

Next we consider the compressed BCHMX case. Here the first reaction is an electrophilic substitution, leading to the intermolecular hydrogen-transfer and NO_2-releasing reaction, as shown in Figure 5. This reaction takes place between two BCHMX molecules in the compressed phase at about 2050 K, and in this reaction one hydrogen atom (H6) of the C3 atom in BCHMX reacts with the N5 atom of the nearby BCHMX to make a new N−H bond via **TS6**, accompanied by forming of the N−H bond, breaking of the N1−N5 bond, and first NO_2^+ being released. This reaction is the rate-determining step (RDS) with a 33.5 kcal/mol barrier, which is 5.0 kcal/mol lower than the intramolecular hydrogen-transfer reaction in uncompressed BCHMX.

As Figure 5 shows, the fragment analysis finds the HONO release reaction pathway at ∼2150 K (13 ps) in Figure 3. In the DFT-MD simulation for the compressed case, the HONO formed from reacting the H of a nearby BCHMX molecule with the NO_2 is ∼3.29 Å from the next BCHMX, whereas the $-NO_2$ that could break to form a free NO_2 molecule is only ∼2.51 Å from the nearby BCHMX (see Figure S3, SI). These differences in the packing for the noncompressed case compared with the compressed case rationalize the observed differences in the initial reaction products for these fast DFT-MD cook-off simulations. This reaction pathway starting from one BCHMX molecule via **TS7** to **Int7** has a lower barrier height of 29.9

DOI: 10.1021/jp510328d
J. Phys. Chem. C 2015, 119, 2290−2296

kcal/mol, with much higher exothermicity of 13.2 kcal/mol, compared to the proposed HONO-releasing reaction in noncompressed BCHMX discussed above. Another similar pathway (via **TS8** to **Int8**) to release HONO in the compressed BCHMX case is also shown in Figure 5, although it is not observed at 2150 K in compressed BCHMX DFT-MD simulation. This possible reaction pathway also has a similar barrier height of 30.5 kcal/mol and with a slightly lower exothermicity of 12.3 kcal/mol. These two pathways have barrier heights 3−4 kcal/mol lower than the proposed HONO release case of noncompressed BCHMX, indicating that pressure facilitates the decomposition of BCHMX. The activation entropy must be included in comparing the rates of reactions at 298.15 K to those at 2000 K. From the finite molecule transition state, we calculate an activation entropy of 5.82 cal/(mol K) for intermolecular H transfer. Thus, the contribution of the activation entropy to the activation free energy is $-\Delta S^*T$ or −11.6 kcal/mol at 2000 K versus −1.74 kcal/mol at 298.15 K. For HONO elimination the finite molecule transition state leads to an activation entropy of 1.66 cal/(mol K). Hence the contribution of the activation entropy to the activation free energy is $-\Delta S^*T$ or −3.32 kcal/mol at 2000 K versus −0.50 kcal/mol at 298.15 K.

4. CONCLUSIONS

We examined the initial chemical reactions of the explosive BCHMX by DFT-MD simulations to discover the reaction steps at high temperature followed by full DFT calculations on a finite cluster to obtain the transition states for the reactions. Key points of the our simulations are

(1) For noncompressed BCHMX, DFT-MD finds that nitro-aci isomerization reaction is first, followed by unimolecular NO_2 release.
(2) For compressed BCHMX (20 GPa), DFT-MD finds that intermolecular hydrogen transfer is first, followed by bimolecular NO_2 release.
(3) For compressed BCHMX, the intermolecular hydrogen-transfer decreases the reaction barrier for releasing NO_2 by ∼7 kcal/mol.
(4) The HONO releasing reaction is more favorable (29.9 kcal/mol barrier) for compressed BCHMX, with a reaction barrier 10 kcal/mol lower than the unimolecular NO_2 releasing reaction and ∼3 kcal/mol lower the than bimolecular NO_2 releasing reaction.

These simulations rationalize the high impact sensitivity of BCHMX, compared to RDX and HMX. It arises because of much lower initial reaction barriers (29.9−33.5 kcal/mol) for BCHMX compared to the 39.0 kcal/mol NO_2 dissociation barrier for RDX[11] and 39.8 kcal/mol NO_2 dissociation barrier for HMX.[17] Thus, the lower initial decomposition barrier for BCHMX explains the higher sensitivity of BCHMX.

We also have used DFT-MD simulations to investigate the initial decomposition reaction of TKX-50[38] and DTTO,[39] which have been predicted to be insensitive energetic materials. Here we find that the first decomposition barrier is lower than 45.1 kcal/mol for TKX-50 and lower than 45.9 kcal/mol for DTTO. Thus, the lower decomposition barrier for BCHMX can explain the higher sensitivity of BCHMX.

In order to decrease the sensitivity of BCHMX, we suggest modifications to avoid the intermolecular hydrogen-transfer and HONO reaction. This can be done by replacing the H atom with a halogen atom such as F or Cl. Also synthesizing the cocrystal combining BCHMX with other EMs, such as HMX, might decrease the sensitivity of energetic materials.[40,41]

■ ASSOCIATED CONTENT

Supporting Information

Atomic coordinates of all intermediates and TS shown in this study, coordinates for structure of BCHMX, and the bond type and bond cutoff in the fragment analysis. This material is available free of charge via the Internet at http://pubs.acs.org.

■ AUTHOR INFORMATION

Corresponding Author

*E-mail: wag@wag.caltech.edu.

Notes

The authors declare no competing financial interest.

■ ACKNOWLEDGMENTS

This research was funded by ONR (N00014-09-1-0634, Cliff Bedford). C.-C. Ye was sponsored by the China Scholarship Council and thanks the Innovation Project for Postgraduates in Universities of Jiangsu Province (Grant No. CXZZ13_0213).

■ REFERENCES

(1) Coon, C. L. In *Proceedings of the International Symposium on Pyrotechnics and Explosives, Proceedings of the International Symposium on Pyrotechnics and Explosives*, Beijing, 1987.
(2) Qiu, L.; Ju, X. H.; Xiao, H. M. Density Functional Theory Study of Solvent Effects on the Structure and Vibrational Frequencies of Tetranitrotetraazabicyclooctane "Bicyclo-HMX". *J. Chin. Chem. Soc.* **2005**, *52*, 405−413.
(3) Koppes, W. M.; Chaykovsky, M.; Adolph, H. G.; Gilardi, R.; George, C. Synthesis and Structure of Some Peri-Substituted 2,4,6,8-Tetraazabicyclo[3.3.0]Octanes. *J. Org. Chem.* **1987**, *52*, 1113−1119.
(4) Pagoria, P. F.; Mitchell, A. R.; Schmidt, R. D.; Coon, C. L.; Jessop, E. S. In *New Nitration and Nitrolysis Procedures in the Synthesis of Energetic Materials*; ACS Symposium Series; ACS: Washington DC, 1996; pp 151−164.
(5) Klasovity, D.; Zeman, S.; Ruzicka, A.; Jungova, M.; Rohac, M. Cis-1,3,4,6-Tetranitrooctahydroimidazo-[4,5-D]Imidazole (BCHMX), Its Properties and Initiation Reactivity. *J. Hazard. Mater.* **2009**, *164*, 954−961.
(6) Gilardi, R.; Flippen-Anderson, J. L.; Evans, R. Cis-2,4,6,8-Tetranitro-1h,5h-2,4,6,8-Tetraaza-Bicyclo[3.3.0]Octane, the Energetic Compound 'Bicyclo-HMX'. *Acta Crystallogr. E* **2002**, *58*, O972−O974.
(7) Yan, Q. L.; Zeman, S.; Svoboda, R.; Elbeih, A. Thermodynamic Properties, Decomposition Kinetics and Reaction Models of BCHMX and Its Formex Bonded Explosive. *Thermochim. Acta* **2012**, *547*, 150−160.
(8) Sikder, A. K.; Bhokare, G. M.; Sarwade, D. B.; Agrawal, J. P. Synthesis, Characterization and Thermal Behaviour of 2,4,6,8-Tetranitro-2,4,6,8-Tetraazabicyclo[3.3.1]Nonane-3,7-Dione (Tnpdu) and One of Its Methylene Analogues. *Propellants, Explos., Pyrotech.* **2001**, *26*, 63−68.
(9) Li, W. J.; Hua, G. F.; Chen, M. O., Synthesis and Properties of 2,4,6,8-Tetranitro-2,4,6,8-Tetraazabicyclo(3,3,0) Octanone-3. *Proceedings of the International Symposium on Pyrotechnics and Explosives*, October 12−15, Beijing, China 1987; pp 187−189.
(10) Goncharov, T. K.; Dubikhin, V. V.; Nazin, G. M.; Prokudin, V. G.; Aliev, Z. G. Thermal Decomposition of Cis-2,4,6,8-Tetranitro-1h,5h-2,4,6,8-Tetraazabicyclo[3.3.0]Octane. *Russ Chem. B*$^+$ **2011**, *60*, 1138−1143.
(11) Chakraborty, D.; Muller, R. P.; Dasgupta, S.; Goddard, W. A., III The Mechanism for Unimolecular Decomposition of RDX (1,3,5-Trinitro-1,3,5-Triazine), an Ab Initio Study. *J. Phys. Chem. A* **2000**, *104*, 2261−2272.

DOI: 10.1021/jp510328d
J. Phys. Chem. C 2015, 119, 2290−2296

(12) Umezawa, N.; Kalia, R. K.; Nakano, A.; Vashista, P.; Shimojo, F. 1,3,5-Trinitro-1,3,5-Triazine Decomposition and Chemisorption on Al(111) Surface: First-Principles Molecular Dynamics Study. *J. Chem. Phys.* **2007**, *126*, 234702.
(13) Fifer, R. A. *Fundamentals of Solid-Propellant Conbustion*; AIAA: New York, 1984; p 90.
(14) Manaa, M. R.; Fried, L. E.; Melius, C. F.; Elstner, M.; Frauenheim, T. Decomposition of Hmx at Extreme Conditions: A Molecular Dynamics Simulation. *J. Phys. Chem. A* **2002**, *106*, 9024−9029.
(15) Han, S. P.; van Duin, A. C.; Goddard, W. A., III; Strachan, A. Thermal Decomposition of Condensed-Phase Nitromethane from Molecular Dynamics from Reaxff Reactive Dynamics. *J. Phys. Chem. B* **2011**, *115*, 6534−6540.
(16) Strachan, A.; Kober, E. M.; van Duin, A. C.; Oxgaard, J.; Goddard, W. A., III Thermal Decomposition of Rdx from Reactive Molecular Dynamics. *J. Chem. Phys.* **2005**, *122*, 54502.
(17) Chakraborty, D.; Muller, R. P.; Dasgupta, S.; Goddard, W. A., III Mechanism for Unimolecular Decomposition of HMX (1,3,5,7-Tetranitro-1,3,5,7-Tetrazocine) an Ab Initio Study. *J. Phys. Chem. A* **2001**, *105*, 1302−1314.
(18) Bulusu, S. N. *Chemistry and Physics of Energetic Materials*; Kluwer Academic: Boston Norwell, MA, U.S.A., 1990; p 764.
(19) Wu, C. J.; Fried, L. E. Ab Initio Study of Rdx Decomposition Mechanisms. *J. Phys. Chem. A* **1997**, *101*, 8675−8679.
(20) Irikura, K. K. Aminoxyl (Nitroxyl) Radicals in the Early Decomposition of the Nitramine RDX. *J. Phys. Chem. A* **2013**, *117*, 2233−2241.
(21) Cohen, R.; Zeiri, Y.; Wurzberg, E.; Kosloff, R. Mechanism of Thermal Unimolecular Decomposition of Tnt (2,4,6-Trinitrotoluene): A DFT Study. *J. Phys. Chem. A* **2007**, *111*, 11074−11083.
(22) Chen, X. F.; Liu, J. F.; Meng, Z. H.; Han, K. L. Thermal Unimolecular Decomposition Mechanism of 2,4,6-Trinitrotoluene: A First-Principles DFT Study. *Theor. Chem. Acc.* **2010**, *127*, 327−344.
(23) Furman, D.; Kosloff, R.; Dubnikova, F.; Zybin, S. V.; Goddard, W. A., III; Rom, N.; Hirshberg, B.; Zeiri, Y. Decomposition of Condensed Phase Energetic Materials: Interplay between Uni- and Bimolecular Mechanisms. *J. Am. Chem. Soc.* **2014**, *136*, 4192−4200.
(24) Wang, B.; Wright, D.; Cliffel, D.; Haglund, R.; Pantelides, S. T. Ionization-Enhanced Decomposition of 2,4,6-Trinitrotoluene (TNT) Molecules. *J. Phys. Chem. A* **2011**, *115*, 8142−8146.
(25) Kim, H.; Choi, J. M.; Goddard, W. A., III Universal Correction of Density Functional Theory to Include London Dispersion (up to Lr, Element 103). *J. Phys. Chem. Lett.* **2012**, *3*, 360−363.
(26) Kohn, W.; Sham, L. J. Self-Consistent Equations Including Exchange and Correlation Effects. *Phys. Rev.* **1965**, *140*, 1133.
(27) Hohenberg, P.; Kohn, W. Inhomogeneous Electron Gas. *Phys. Rev. B* **1964**, *136*, B864.
(28) Kresse, G.; Furthmuller, J. Efficient Iterative Schemes for Ab Initio Total-Energy Calculations Using a Plane-Wave Basis Set. *Phys. Rev. B* **1996**, *54*, 11169−11186.
(29) Kresse, G.; Furthmuller, J. Efficiency of Ab-Initio Total Energy Calculations for Metals and Semiconductors Using a Plane-Wave Basis Set. *Comput. Mater. Sci.* **1996**, *6*, 15−50.
(30) Kresse, G. Ab-Initio Molecular-Dynamics for Liquid-Metals. *J. Non-Cryst. Solids* **1995**, *193*, 222−229.
(31) Bochevarov, A. D.; Harder, E.; Hughes, T. F.; Greenwood, J. R.; Braden, D. A.; Phillipp, D. M.; Rinaldo, D.; Halls, M. D.; Zhang, J.; Friesner, R. A. Jaguar: A High-Performance Quantum Chemistry Software Program with Strengths in Life and Materials Sciences. *Int. J. Quantum Chem.* **2013**, *113*, 2110−2142.
(32) Bowden, F. P.; Yoffe, A. D. *Initiation and Growth of Explosions in Liquids and Solids*; Cambridge University Press: Cambridge, UK, 1952.
(33) An, Q.; Zybin, S. V.; Goddard, W. A., III; Jaramillo-Botero, A.; Blanco, M.; Luo, S. N. Elucidation of the Dynamics for Hot-Spot Initiation at Nonuniform Interfaces of Highly Shocked Materials. *Phys. Rev. B* **2011**, *84*, 220101.
(34) An, Q.; Goddard, W. A., III; Zybin, S. V.; Jaramillo-Botero, A.; Zhou, T. T. Highly Shocked Polymer Bonded Explosives at a Nonplanar Interface: Hot-Spot Formation Leading to Detonation. *J. Phys. Chem. C* **2013**, *117*, 26551−26561.
(35) An, Q.; Goddard, W. A., III; Zybin, S. V.; Luo, S.-N. Inhibition of Hotspot Formation in Polymer Bonded Explosives Using an Interface Matching Low Density Polymer Coating at the Polymer-Explosive Interface. *J. Phys. Chem. C* **2014**, *118*, 19918−19928.
(36) Minier, L. M.; Brower, K. R.; Oxley, J. C. Role of Intermolecular Reactions in Thermolysis of Aromatic Nitro-Compounds in Supercritical Aromatic Solvents. *J. Org. Chem.* **1991**, *56*, 3306−3314.
(37) Davis, L. L.; Brower, K. R. Reactions of Organic Compounds in Explosive-Driven Shock Waves. *J. Phys. Chem.* **1996**, *100*, 18775−18783.
(38) An, Q.; Liu, W.-G.; Goddard, W. A., III; Cheng, T.; Zybin, S. V.; Xiao, H. Initial Steps of Thermal Decomposition of Dihydroxylammonium 5,5′-Bistetrazole-1,1′-Diolate Crystals from Quantum Mechanics. *J. Phys. Chem. C* **2014**, *118*, 27175−27181.
(39) Ye, C.-C.; An, Q.; Goddard, W. A., III; Cheng, T.; Liu, W.-G.; Zybin, S. V.; Ju, X.-H. Initial Decomposition Reaction of Di-Tetrazine-Tetroxide (DTTO) from Quantum Molecular Dynamics: Implications for a Promising Energetic Material. *J. Mater. Chem. A* **2015**, DOI: 10.1039/c4ta05676k.
(40) Landenberger, K. B.; Matzger, A. J. Cocrystals of 1,3,5,7-Tetranitro-1,3,5,7-Tetrazacyclooctane (HMX). *Cryst. Growth Des.* **2012**, *12*, 3603−3609.
(41) Bolton, O.; Simke, L. R.; Pagoria, P. F.; Matzger, A. J. High Power Explosive with Good Sensitivity: A 2:1 Cocrystal of CL-20:HMX. *Cryst. Growth Des.* **2012**, *12*, 4311−4314.

DOI: 10.1021/jp510328d
J. Phys. Chem. C 2015, 119, 2290−2296